JOURNAL OF GEOPHYSICAL RESEARCH, VOL. 103, NO. A12, PAGES 29,267–29,275, DECEMBER 1, 1998

Propagation of medium frequency (1–4 MHz) auroral radio waves to the ground via the Z-mode radio window

Peter H. Yoon, A. T. Weatherwax, and T. J. Rosenberg

Institute for Physical Science and Technology, University of Maryland, College Park

J. LaBelle and S. G. Shepherd

Department of Physics and Astronomy, Dartmouth College, Hanover, New Hampshire

Abstract. Recent ground-based observations of auroral radio waves have identified narrowband emissions near 2 and 3 times the lower ionospheric electron cyclotron frequency (f_{ce}) known as auroral roars. In this paper the propagation of these waves in the auroral ionosphere is investigated by means of a ray-tracing technique. We model one particular scenario in which a large-scale (tens of kilometers) horizontal density structure, based on density structures observed with the Sondrestrom radar at times of auroral roar emissions, plays a crucial role in both guiding the waves to the ground and enabling mode conversion. The location and the mode characteristics of the initial waves are determined on the basis of local stability properties, which suggests that Z-mode wave excitation is favored near $2f_{ce}$. However, since Z-mode cannot propagate to the ground they must first undergo a mode conversion to one of the free-space modes (X and O). It is found that for a narrow range of frequencies and initial wave phase angles the trapped Z mode can be converted to O mode via the Ellis radio window. This finding is consistent with the fact that auroral roar emissions are nearly 100% O-mode polarized. However, it is important to note that the evaluation of the damping of the Z-mode waves along the ray path is not considered within the context of this preliminary study and will be critical for eventually determining the exact physical scenario of the auroral roar generation mechanism.

1. Introduction

Recent ground-based studies of auroral radio emissions at 1–4 MHz frequency range have revealed new and interesting phenomena. These include narrowband emissions in the vicinity of the first ($2f_{ce}$) and second ($3f_{ce}$) harmonics of the lower ionospheric electron cyclotron frequency at the source location [*Kellogg and Monson,* 1979, 1984; *Weatherwax et al.,* 1993, 1995; *Hughes and LaBelle,* 1998; *LaBelle and Weatherwax,* 1992]. Here $f_{ce} = \Omega_{ce}/2\pi = eB/2\pi m_e c$ is the local electron cyclotron frequency with B being the intensity of the geomagnetic field at F region ionospheric heights. These emissions, together with auroral hiss, are often precursors to the expansion phase of auroral substorms [*LaBelle et al.,* 1994; *Weatherwax et al.,* 1995]. Observations have also revealed that these emissions consist of hundreds of fine frequency structures [*LaBelle et al.,* 1995; *Shepherd et al.,* 1998a]. Recently, *Shepherd et al.* [1998b] observed that the $2f_{ce}$ auroral roar waves are predominantly O-mode polarized.

Weatherwax et al. [1995] first provided rough estimates of direct maser-type growth rates for both $2f_{ce}$ and $3f_{ce}$ X modes and showed that they could exceed the ionospheric collisional damping rate, although growth rates were low. However, recent observational [*Shepherd et al.,* 1998b] and theoretical [*Willes et al.,* 1998] works suggest that an X-mode maser is not a viable roar emission generation mechanism. *Weatherwax et al.* [1995] also speculated on the possibility of indirect radiation mechanisms which include nonlinear wave-wave coalescence of two Z modes (at f_{ce}) into either of the two free-space modes (X or O) to produce $2f_{ce}$ emissions and linear mode conversion of Z mode into O mode. The latter mechanism is known as the "Ellis radio window" mechanism [*Ellis,* 1956].

In order to reassess the direct emission mechanism for free-space modes, *Yoon et al.* [1996] worked out a detailed instability analysis for X and O modes under physical parameters typical of the auroral roar source region. Meanwhile, *Willes et al.* [1998] discussed the nonlinear coalescence theory in a quantitative manner. On the basis of Z-mode propagation path, they showed

Paper number 1998JA900032.
0148-0227/98/1998JA900032$09.00

that repeated coalescences of Z modes are indeed a possibility. Their study is similar to that of an earlier one by *Melrose* [1991] in the solar context. More recently, *Yoon et al.* [1998] reassessed the maser growth rate calculation including the Z mode and showed that the growth rates of Z mode at $2f_{ce}$ ($Z2$) and $3f_{ce}$ ($Z3$) are greatly enhanced when the ionospheric condition is such that the local upper hybrid frequency matches the harmonics of electron cyclotron frequency,

$$f_{uh}^2 = f_{ce}^2 + f_{pe}^2 = (s\, f_{ce})^2 \quad s = 2 \text{ and } 3$$

Here $f_{pe} = \omega_{pe}/2\pi = (n_e e^2/\pi m_e)^{1/2}$ is the local electron plasma frequency, n_e being the number density. This finding is consistent with rocket flight observations of intense electrostatic upper hybrid waves when the said matching condition is met [*Cartwright and Kellogg,* 1974; *Gough and Urban,* 1983; *Gough et al.,* 1995; *McFadden et al.,* 1986], and also agrees with earlier theoretical findings by *Kaufmann* [1980], *Winglee and Dulk* [1986a, 1986b] and *Benson and Wong* [1987]. However, since the Z mode is a trapped mode a conversion into one of the free space modes is necessary in order for the excited waves to reach the ground [*Gough and Urban,* 1983; *Weatherwax et al.,* 1995].

One candidate escape mechanism involves linear mode conversion of Z mode into either O or W (whistler) mode, i.e., the Ellis radio window mechanism. Such an idea has its origin from early studies of radio wave propagation in the ionosphere [e.g., *Ellis,* 1956]. The purpose of the present article is to investigate the Ellis radio window mechanism in the context of auroral roar emissions in a quantitative manner by means of a ray-tracing technique.

The organization of the present paper is as follows: In section 2, we introduce the model of bottomside auroral ionosphere, which will be used in the ray-tracing calculation. Section 3 presents the results of the ray-tracing calculation carried out over the model ionosphere. Finally, section 4 concludes the discussion.

2. Model of Bottomside Auroral Ionosphere

The auroral ionosphere at F region altitudes is characterized by pervasive horizontal density structures [*Brinton et al.,* 1978; *Tsunoda,* 1988; *Kelley,* 1989; *Rodger et al.,* 1992; *Doe et al.,* 1993, 1995]. *Shepherd et al.* [this issue] report that the typical ionospheric electron density during the roar emission (measured with incoherent scatter radar technique) is characterized with horizontal structures of a few tens of kilometers. On this basis we model our electron density as a function of both the altitude z and one horizontal spatial coordinate, say x.

Figure 1 displays the contour plots of the total electron number density $n_e(x,z)$ (Figure 1a) and the ratio f_{pe}/f_{ce} (Figure 1b) versus horizontal distance x and altitude z. In Figure 1b, we also superpose the gray-scale plot of the maximum growth rates for the $Z2$ and $O1$ modes. The $Z2$ mode growth rate corresponds to the higher-altitude range, while the narrow band of light shades in the lower-altitude region corresponds to the $O1$-mode growth region. The $Z2$ growth rate is generally higher than that of $O1$, as evidenced by the darker shades. Unshaded regions correspond to wave absorption regions (either by collisionless cyclotron damping or by electron/ion, electron/neutral collisional damping).

The computation of the local maximum growth rate is based upon the recent paper by *Yoon et al.* [1998] in which a small population of energetic electrons possessing a downgoing beam feature (with $\sim$10 keV beam kinetic energy) and upgoing loss-cone feature is assumed to exist along the auroral field lines. The thermal energy of these electrons is assumed to be $\sim$1 keV. Their number density is generally small in comparison with that of the background (diffusive equilibrium) electrons at F region altitudes. In the present model the number density of the energetic electrons is simply taken to be of the form

$$n_{energ}(x,z) = 10^{-3}\, n_e(x,z)\, \mathrm{sech}^2(x/L) \qquad (1)$$

which implies that the highest concentration of energetic electrons is in the near vicinity of the center of the structure, $x = 0$ (this is why the shades turn progressively lighter as one moves away from $x = 0$).

According to *Yoon et al.* [1998], for the range of frequency ratios corresponding to $f_{pe}/f_{ce} < 1$ or so the excitation of $O1$, $X2$, and $Z1$ waves are favored, which is why the $O1$-mode growth occurs only for low-altitude regions near 100–125 km for which f_{pe}/f_{ce} is less than unity. $Z1$ and $X2$ maximum growth rates are not plotted.

For f_{pe}/f_{ce} greater than unity, *Yoon et al.* [1998] find that $Z2$ and $Z3$ modes are favorably excited. Specifically, for a rough range corresponding to $\sqrt{3} < f_{pe}/f_{ce} \leq 2.25$. the $Z2$ mode possesses a high maximum growth rate (with a peak near $f_{pe}/f_{ce} \approx \sqrt{3} \sim 1.73$). Similarly, for $\sqrt{8} < f_{pe}/f_{ce} \leq 3.2$ or so, the $Z3$ mode has a high maximum growth rate with the peak near $f_{pe}/f_{ce} \approx \sqrt{8}$. These peaks, of course, correspond to the upper hybrid frequency matching condition $f_{pe}^2 + f_{ce}^2 = (sf_{ce})^2$ ($s = 2$ and 3), mentioned earlier.

Indeed, the $Z2$-mode growth rate represented by gray scale indicates that intense excitation of $Z2$-mode waves occurs for $f_{pe}/f_{ce} \geq \sqrt{3}$. It is interesting to note, however, that the most intense $Z2$-mode growth occurs for f_{pe}/f_{ce} slightly above the exact matching value $\sqrt{3} \approx 1.73$. Note that for the present choice of background electron temperature ($T_{de} = 10^3$ K) the resulting ratio f_{pe}/f_{ce} is too low to excite the $Z3$ mode, which requires a higher f_{pe}/f_{ce} ($> \sqrt{8}$). As a consequence, the present study is relevant only to the $2f_{ce}$ roar emissions. However, we hasten to point out that the present study can be easily generalized for the discussion of $3f_{ce}$ emissions. If we choose lower T_{de} (say, $\sim$ 950 K, for in-

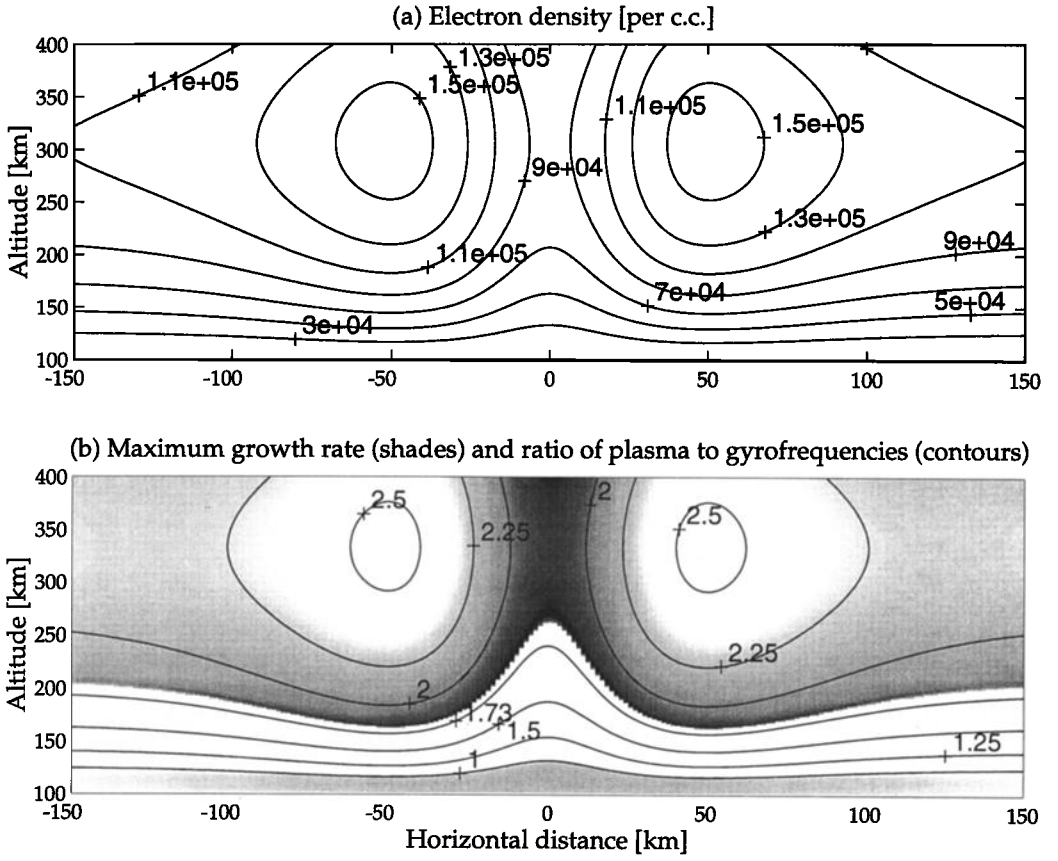

Figure 1. Contour plots of (a) the total electron density $n_e(x, z)$ and (b) the ratio $f_{pe}(x, z)/f_{ce}(z)$ versus the horizontal distance x and altitude z. In Figure 1b the maximum growth rates for the $Z2$ and the $O1$ modes are also superposed using gray scale. The much darker region which occupies a much larger, high-altitude domain corresponds to the $Z2$ mode, while a narrow band of lighter shades which occupy the lower altitudes just above 100 km corresponds to the O mode.

stance), we can easily obtain higher values of f_{pe}/f_{ce} for which $Z3$-mode excitation is favored over $Z2$-mode excitation.

In the ray-tracing calculation to follow we initialize the rays according to the local $Z2$-mode growth properties, as indicated by the gray-scale representation of the maximum growth rate. The local growth rate property also reveals that the phase angle for the most unstable modes is invariably a 90° propagation angle [*Yoon et al.*, 1996]. Therefore, initial rays are all launched with phase angle θ close to 90°. We assume that the initial waves are close to twice the local electron gyrofrequency:

$$f = s\, f_{ce} \approx 2.80\, s\, B(z)\,[\mathrm{MHz}] \qquad (2)$$

where $B(z)$ is given by (A5) (see Appendix A) and $s = 1.995$. The reason an exact integer $s = 2$ is not used is again due to the local stability property, which shows that $2f_{ce}$ waves are excited just below an exact integer harmonic [*Yoon et al.*, 1996]; $s = 1.995$ is a good representative value. By assuming the relation (2) the launch frequency is automatically determined once we choose the launch height z. For a given z we then survey the x space for the highest maximum growth rate. For altitudes above $\sim$ 250 km, $x = 0$ marks the location for which the most intense $Z2$ mode is excited, but below $\sim$ 250 km altitude the highest $Z2$ growth occurs not at $x = 0$ but at some distance away in either direction. Our numerical scheme automatically finds the most unstable x location.

3. Ray-Tracing Analysis

The Z mode is a trapped mode in cold magnetoionic plasma ray theory. Therefore, if we simply follow the Z-mode ray path, the mode eventually becomes a nonpropagating mode (that is, the index of refraction N approaches infinity, and the group velocity becomes zero). At this point the wave energy will be absorbed back by the ambient plasma. However, according to Ellis radio window theory, a portion of the Z-mode wave energy can be converted to that of the O mode, provided the wave phase vector becomes nearly parallel to the ambient field ($\sin\theta \approx 0$), frequency f is sufficiently close to the local plasma frequency f_{pe}, and the index of refraction, N^2, becomes sufficiently close to a critical value N^2_{cr}, where

$$N^2_{cr} = f_{ce}/(f_{ce} + f_{pe}) \qquad (3)$$

The concept of Ellis radio window is quite straightforward, and it can be understood on the basis of the magnetoionic dispersion relation

$$N^2 = 1 - \frac{T f_{pe}^2}{f\,(Tf - f_{ce}|\cos\theta|)} \tag{4}$$

where $T = (f_{pe}^2 - f^2)(s \pm \sqrt{1+s^2})/|f^2 - f_{pe}^2|$, and $s = f f_{ce} \sin^2\theta/2\,|f^2 - f_{pe}^2|\,|\cos\theta|$. Here the plus or minus corresponds to X/Z and O/W mode, respectively. For $f_{pe}/f_{ce} < 1$ the Z mode branch and the O and W modes share the same values of the refractive index at two points when $\theta = 0$. These points of intersection correspond to the exact Ellis window, where the transmission coefficient of Z to either O or W and vice versa are 100% (the calculation of intensity transmission coefficient is not so straightforward, however, and involves the solution of mode conversion differential equation). The point that allows Z- to W-mode conversion is called the first Ellis window, while the other point for Z- to O-mode conversion is the second Ellis window. The squares of indices of refraction at the first and second Ellis windows are given by

$$N_{cr1}^2 = \frac{f_{ce}}{f_{ce} - f_{pe}} \quad N_{cr2}^2 = \frac{f_{ce}}{f_{ce} + f_{pe}} \tag{5}$$

respectively. For the case of $f_{pe}/f_{ce} > 1$, the first Ellis window does not exist, but only the second window remains as a mode conversion channel. The critical index of refraction (3) thus corresponds to the second Ellis window.

The distance ds between a point in a three-dimensional parameter space $(f/f_{ce}, \sin\theta, N^2)$ and the exact Ellis window point $(f_{pe}/f_{ce}, 0, N_{cr}^2)$ is given by

$$(ds)^2 = \sin^2\theta + (f - f_{pe})^2/f_{ce}^2 + (N^2 - N_{cr}^2)^2 \tag{6}$$

If $ds = 0$, a mode is in the exact Ellis window, where the Z- to O-mode conversion is 100%. However, partial conversion is possible even if ds is finite as long as it is sufficiently small. *Smith* [1973] numerically estimates the angular width of the Ellis window to be $\sim 6°$ on the basis of the half width of the intensity transmission coefficient. The *Smith* [1973] calculation, and other related early works, are relevant for ionospheric radio wave propagation problems, assuming a simple one-dimensional stratefied density inhomogeneity. Our problem is more complicated in that we must deal with at least a two-dimensional spatial gradient. To simplify the matter, we do not attempt to calculate the width of the radio window from first principle, but simply extrapolate these early results for our need.

To implement the Ellis window access condition in our ray-tracing code, we have first numerically tabulated the quantity ds defined in (6) as a function of both the frequency f and the angle θ, varying the ratio f_{pe}/f_{ce} as an input parameter. For a wide range of f_{pe}/f_{ce} we found that the minimum distance between a point $(f/f_{ce}, \sin\theta, N^2)$ when θ is 3° (thus, 6° width), and the Ellis window point $(f_{pe}/f_{ce}, 0, N_{cr}^2)$ is approximately given by $ds \sim 0.054$. Generally, we also found that the minimum distance ds and the angular width $d\theta$ scale linearly as $ds \sim 0.054\,d\theta/6$, where $d\theta$ is given in degree. Armed with this information, we first specify a permissible Ellis window width $d\theta_E$ (measured in degree) in the ray-tracing code. Then as we calculate the ray path, we evaluate ds at each point. In general, if a mode is far from the Ellis window, ds is large. However, as the mode approaches the Ellis window, ds decreases in magnitude. If

$$ds \le 0.054\,d\theta_E/6 \tag{7}$$

then we stop the calculation and declare that the mode has accessed the Ellis radio window.

In Figure 2 we present some sample $Z2$ mode ray paths, superposed on top of the gray-scale maximum growth rate plot. Figure 2a shows five different launch heights, which include $z = 350$ (2772.2 kHz), 325 (2803.4 kHz), 300 (2835 kHz), 275 (2899.7 kHz), and 250 km (2867 kHz). Initial ray positions along x are all located at $x = 0$, since $x = 0$ corresponds to the highest $Z2$ maximum growth rate for a given z (darkest shade), except for 250 km case (or 2867 kHz). For the case of 250 km the maximum growth occurs some distance away from $x = 0$ on either side. Therefore the ray is launched to the left of $x = 0$ where the highest wave growth takes place (which is determined automatically in the code). Launch angles are $\theta(0) = 90°$ for all cases. Of the five cases considered, only the ray launched at 300 km eventually accesses the Ellis radio window (beyond which, the mode presumably converts to O mode). This case is shown with a solid line, while other cases are depicted with dashes. The final location where the ray hits the radio window is designated with a small circle. In this calculation the predesignated angular width of the radio window is $d\theta_E = 6°$ [*Smith*, 1973]. For those modes that do not access the radio window the waves eventually evolve into nonpropagating modes.

In Figure 2b, we show the $Z2$ mode ray paths with a fixed initial location ($x = 0$, $z = 300$ km, which corresponds to 2835 kHz) but with a slight variation in launch angles. The local growth theory [*Yoon et al.*, 1996] predicts that $\theta = 90°$ corresponds to the highest wave growth, with the growth rate rapidly decreasing as one moves away from the exactly perpendicular direction. Significant wave growth occurs only within 5° in each direction about the 90° angle. In this regard the 80° and 100° cases depicted in the figure have already been stretched somewhat beyond the limit. Of the five different launch angles, two cases eventually reach the Ellis window (and convert to O-mode waves). Note that the mode launched with 80° phase angle converts to an upward propagating O mode and thus cannot reach the ground, whereas the mode launched at 90° is directed toward the ground.

For the particular parameters modeled here the Z mode waves are refracted away from the high density

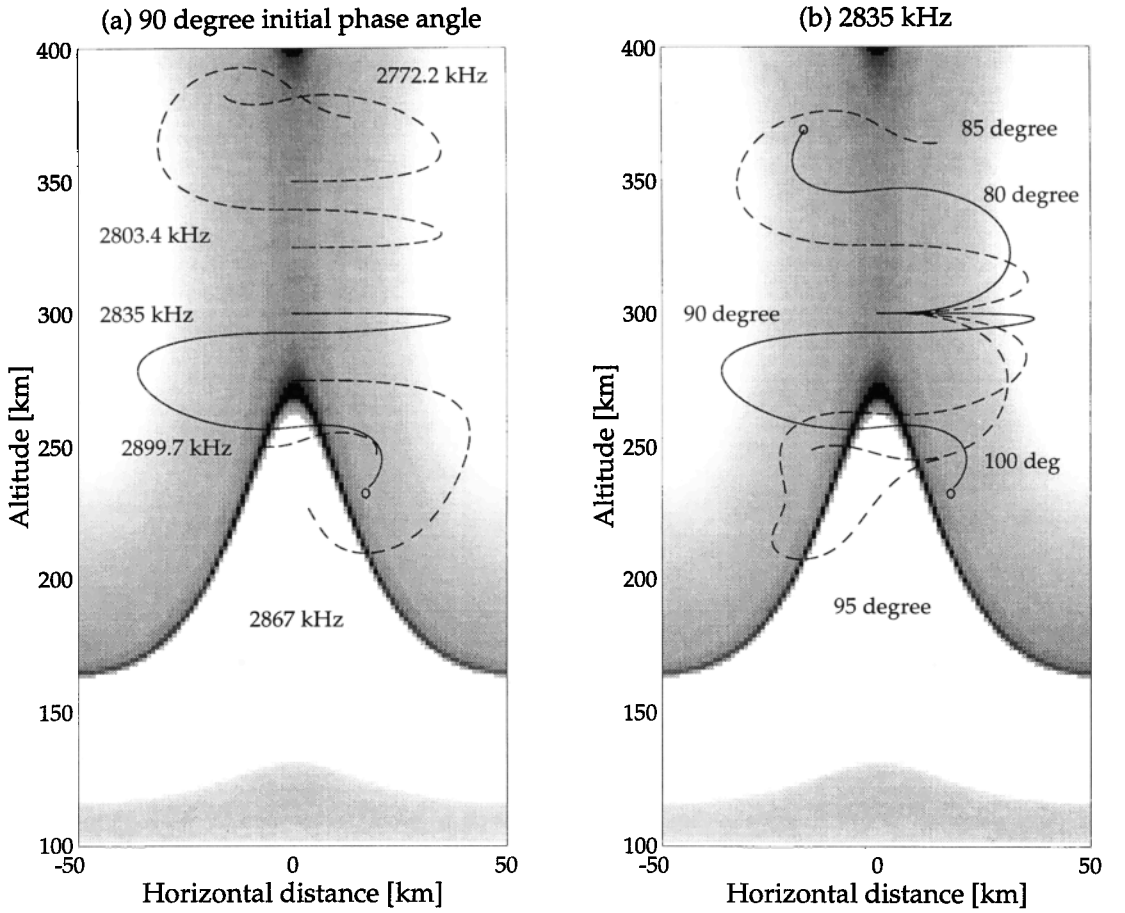

Figure 2. (a) The $Z2$-mode ray paths for various launch altitudes, which includes $z = 350$, 325, 300, 275, and 250 km. Assuming the relation $f = 1.995\, f_{ce}$, the corresponding frequencies are 2772.2, 2803.4, 2835, 2899.7, and 2867 kHz. The initial location of the rays in x are all at zero (corresponding to the most intense wave emission), except for 250 km, for which the highest wave emission should occur on either sides of $x = 0$. Of the cases shown, only the 2835-kHz wave reaches the Ellis window (shown with solid line, ending with a small circle which marks the location at which the ray hits the Ellis window). (b) The ray paths of 2835-kHz mode launched with several different phase angles. Of the various cases considered the rays launched at 80° and 90° initial phase angles are capable of accessing the radio window and thus partly converting to O mode. These two cases are shown with solid lines.

and are in effect guided by the density cavity. However, the propagation is sensitive to parameters such as the relation of the wave frequency to $2f_{ce}$, particularly if warm plasma effects are included. Other regimes exist in which the waves are confined in density enhancements rather than refracted away from them [e.g., *Ergun*, 1989].

Another way to illustrate the Ellis radio window mechanism is to plot two quantities, $\sin^2\theta$ and $|N^2 - N_{cr}^2|$, as functions of time (in μs). In Figure 3, we plot $\sin^2\theta$ and $|N^2 - N_{cr}^2|$ for the five different cases of initial launch altitudes as shown in Figure 2. A given ray can be considered accessible to the radio window only if $N^2 - N_{cr}^2$ and $\sin^2\theta$ become simultaneously close to zero along the ray path. (The other condition of $f - f_{pe} \sim 0$ follows automatically and thus is not shown.) The only case in Figure 2 for which the ray reaches the Ellis window, namely, 300 km, is plotted with solid lines, while other cases are plotted with dashes. For the 300 km case the quantities $\sin^2\theta$ and $|N^2 - N_{cr}^2|$ indeed become zero at the end of the calculation.

We next consider a continuous variation of the launch height (and therefore the frequency) and the launch angle and investigate the Ellis window accessibility condition in a systematic way. Specifically, we vary the launch height from 325 to 275 km, which corresponds to the frequency range of $\sim$ 2805–2865 kHz. The initial x location is 0 for all cases. For each launch height we continuously vary the initial phase angle from 85° to 95°. In the first run we allow a rather stringent Ellis window access condition. We declare that the mode has accessed the radio window and save the initial frequency and phase angle as output data only if the ray path leads to within 1° of the exact Ellis window. The result is shown in Figure 4a, which plots the launch frequency versus the initial phase angle. We have also run two

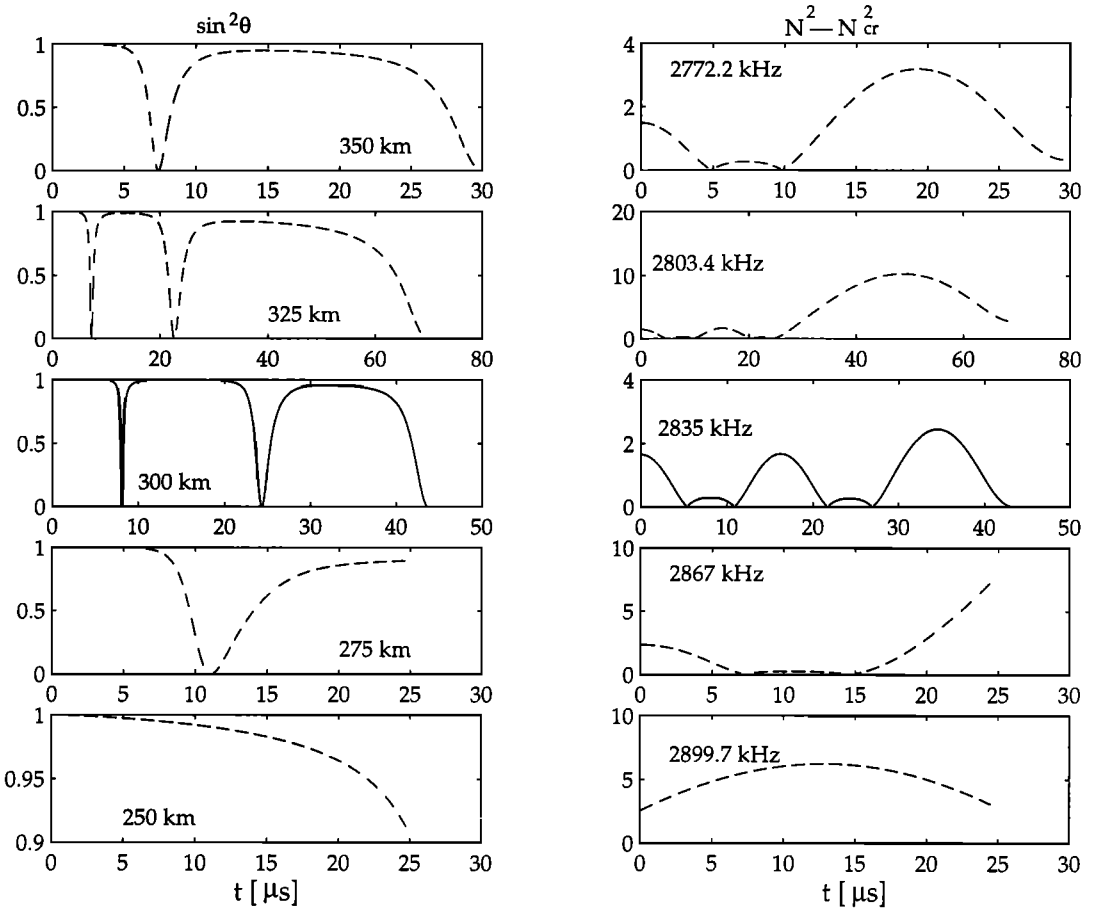

Figure 3. An alternative representation of ray-tracing results, in which $\sin^2\theta$ and $N^2 - N_{cr}^2$ along the ray paths are plotted against time. The cases shown here correspond to the rays shown in Figure 2a. Note that for the 2835 kHz case (or 300 km altitude) the two quantities become zero simultaneously at the end of the calculation, thus demonstrating that the rays have indeed hit the Ellis radio window. For those rays that do not reach the Ellis window the index of refraction N^2 eventually becomes ∞. For those cases we have stopped the calculation before N^2 becomes too large for graphical purposes; otherwise, detailed features for $N^2 - N_{cr}^2$ will be lost because of the large range of the vertial scale.

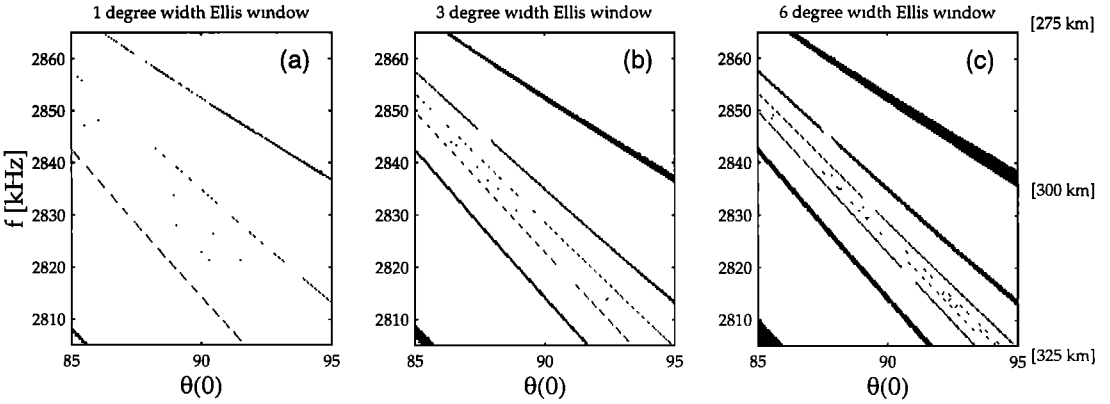

Figure 4. A systematic survey of launch frequency (or equivalently, the altitude) and initial phase angle results in several narrow strips and dots in two-dimensional space (f, θ), which correspond to the initial condition which eventually lead to rays reaching the Ellis window. Note how the widths of the strips progressively widen as an increasingly larger predetermined angular width for the Ellis window is used.

more cases in which we allow the Ellis window to have 3° and 6° angular widths, respectively. These results are shown in Figures 4b and 4c. Figure 4 shows several strips and dots of launch frequency and initial phase angle for which the initial Z mode eventually accesses the Ellis window. As expected, the strips progressively widen as the Ellis window condition is successively relaxed.

4. Conclusions and Discussion

We have modeled one particular possible ionospheric electron density structure characterized by a density depletion (or cavity) at the center and a pair of enhanced ionization patches adjacent to the cavity. The wave source is within the cavity region. Depending on plasma parameters, the waves may be refracted either toward or away from density gradients. For the parameters modeled here using cold plasma theory for the background plasma the waves are refracted away from the density enhancements, so that the cavity structure directs the wave propagation toward the ground. In fact, we find that if we lower the maximum electron concentration from 1.5×10^5 (see Figure 1a) to something like 1.1×10^5, then the Z mode is not confined to the cavity region but propagates out of the source region without much refraction/deflection.

We have also considered the local properties of the source region. One of the most important considerations is the growth rate associated with various magnetoionic modes at the source. In determining the growth rate the local ratio of plasma frequency to electron cyclotron frequency, f_{pe}/f_{ce} plays the major role. For the present model, $Z2$ mode should have the highest wave growth rate inside the source altitude of $\sim$ 275–325 km. We have thus superposed the maximum growth rate of $Z2$ mode in gray scale.

In accordance with the maximum growth condition we have then carried out the ray-tracing calculation and have shown that under right initial condition, $Z2$ mode can convert to O mode by the Ellis radio window mechanism. The initial condition for Ellis window accessibility is surveyed in a plot of initial wave phase angle and the launch frequency (or equivalently, the altitude). The result is a series of narrow strips and dots in angle-frequency space, which allows for the Z-mode waves to eventually access the Ellis window.

The field strengths of auroral roar emissions observed at ground level range from a few μV/m to a few tens of μV/m. The few reported rocket measurements of upper hybrid waves at altitudes above 200 km in the auroral ionosphere are consistent with field strengths the order of tens of mV/m [*Mallinckrodt,* 1980; *Gough and Urban,* 1983]. These ionospheric measurements are not only space- and time-averaged but also represent a meager sampling; larger-amplitude upper hybrid waves may well occur. Nevertheless, using these experimental bounds implies a ratio of at least 10^3–10^4 between the wave field strengths observed in the ionosphere and those observed at ground level. The mechanism described in this paper predicts both wave populations, and four effects may explain the difference in their field strengths: (1) the finite transmission width of the Ellis window, shown in Figures 2 and 4, implies that only a fraction of the Z (or upper hybrid) waves in the ionosphere convert to O mode; (2) as they propagate away from their source, the ionospheric Z-mode waves refract into conditions for which they damp on the surrounding plasma rather than extracting energy from it, so the average Z-mode wave amplitude observed over a volume including the source will in general imply a larger field strength than that which actually characterizes the waves that reach the Ellis window; (3) the O mode experiences absorption as it propagates to the ground, particularly if a dense E region underlies the source; and (4) the O-mode field strength decreases as the wave propagates to ground level because the waves spread out spatially.

We can roughly estimate this spatial spreading of the O-mode waves. The sizes of the density cavities in the auroral zone such as those modeled in Figure 1 as the source region of the waves are typically the order of tens of kilometers; on the other hand, there is evidence from spatially separated ground level measurements that the auroral roar emissions often illuminate regions on the ground of the order of hundreds of kilometers. (Canadian radio observatories spaced 200 km apart often observe common signals.) Therefore we expect a reduction in Poynting flux of the order of 100 because of the spatial spreading, implying a factor of 10 in field strength.

From Figure 4 we can roughly estimate the fraction of wave energy at the source that eventually ray traces to the Ellis window, assuming no absorption and assuming a transmission window of a fixed angular width. This fraction is approximately 1% for the 3°-wide Ellis window, implying another factor of 10 for the ratio of the field strengths. Between them, effects (1) and (4) therefore explain a factor of 10^2 of the observed ratio 10^3–10^4 between the field strength in the ionosphere and that at ground level. This leaves a factor of at least 10–100 to be accounted for by absorption of the waves.

Assuming that fairly weak damping occurs ($\gamma < 0.1\, f$ or so, where γ represents the damping rate), absorption of one or two e foldings seems reasonable in the ionosphere, where the waves propagate for tens of wave periods before hitting the Ellis window (Figure 3). Attenuation of the order of 10^{-1} in field strength (10^{-2} in power) of the O-mode waves between the ionosphere and the ground is quite reasonable considering the high attenuation of these frequencies in the enhanced auroral E region [*Gough and Urban,* 1983]. These two absorption effects are quite difficult to model and are beyond the scope of this paper, but their calculation represents an obvious next step in assessing the feasibility of the mechanism proposed here for explaining auroral roar emissions.

Even if the Z-mode damping turns out to be excessive for the particular scenario modeled by ray tracing

in this paper, there may be other scenarios in which the Z mode avoids damping but still reaches the Ellis window criterion. The modeling in this paper establishes that the Ellis window is a conversion mechanism worth considering when developing theories of the generation of auroral radio emissions.

Appendix A: Model of Bottomside Auroral Ionosphere

The present electron density model is the following:

$$n_e(x,z) = n_0\, n_{\rm de}(z)\, n_{\rm li}(z)\, n_{\rm hs}(x) \tag{A1}$$

where $n_0 = 3.48 \times 10^3\ {\rm cm}^{-3}$ is a reference number density at a reference altitude $z_0 = 10^3$ km. The factor $n_{\rm de}(z)$ is the normalized diffuse equilibrium electron density [*Kimura*, 1966; *Inan and Bell*, 1977; *Horne*, 1995] given by

$$n_{\rm de}(z) = \Big\{ \sum_{i=1}^{N} \eta_i \exp[-G(z)/H_i] \Big\}^{1/2} \tag{A2}$$

where $\eta_1 = 0.3$, $\eta_2 = 0.4$, and $\eta_3 = 0.3$, respectively; $G(z) = (R_E + z_0)(z - z_0)/(R_E + z)$, $R_E = 6370$ km being the Earth radius; and $H_1 = 1.1264\, T_{\rm de}$ km, $H_2 = 0.2816\, T_{\rm de}$ km, and $H_3 = 0.0704\, T_{\rm de}$ km, respectively, $T_{\rm de}$ being the diffuse equilibrium electron temperature. For the present purpose we choose $T_{\rm de} = 10^3$ K, which is typical of the lower ionosphere in the auroral zone.

The factor $n_{\rm li}(z)$ is the lower ionospheric correction term:

$$n_{\rm li}(z) = \frac{\Theta(z - z_M)}{1 + \tanh(z_F - z_M)/H} \times \big[\tanh(z - z_F)/H + \tanh(z_F - z_M)/H\big] \tag{A3}$$

where $\Theta(t) = 1$ for $t > 0$ and zero otherwise; $z_M = 100$ km is the bottom of the ionosphere, below which is presumed to be dominated by the neutral atmosphere; and H and z_F are two adjustable parameters that determine the elevation of the F region peak. For the present purpose we choose $H = 200$ km and $z_F = 400$ km, which place the F region peak at $\sim$300 km. Of course, the F region peak varies from day to night, season to season, and depends on solar conditions. The specific choice is not very important for the present purpose.

Finally, the term $n_{\rm hs}(x)$ represents the horizontal density structure factor:

$$n_{\rm hs}(x) = \Big[1 - \frac{a+b}{1+a} \exp\Big(-\frac{x^2}{L^2}\Big)\Big] \Big(1 + a\, {\rm sech}^2\, \frac{x}{L}\Big) \tag{A4}$$

where L is the half width of the cavity along the x direction and $a(>0)$ and $b(0 < b < 1)$ are two shape parameters. Parameter a controls the degree of symmetric density enhancements centered about $x = 0$, while b determines the degree of density depletion with maximum at $x = 0$ (note that $n_{\rm hs}(0) = 1 - b$). Thus, if $a > 0$ and $b = 0$, then the depression at the center of the structure is absent. In this case the horizontal structure can be characterized by a pair of enhanced ionization patches centered around $x = 0$. On the other hand, if $a = 0$ but b is finite, then the structure can be characterized as a pure density cavity. In the present model we find that the choice of $L = 50$ km, $a = 2.5$, and $b = 0.2$ qualitatively models the typical measured electron density structure.

Finally, the geomagnetic field intensity is modeled by the standard dipole field, given by

$$B(z) = 0.3\,(1 + z/R_E)^{-3}\,(1 + 3\,\sin^2\theta_L)^{1/2} \tag{A5}$$

where θ_L represents the latitude angle (we choose $\theta_L \approx 74°$) and the unit for B is gauss. Plasma frequency and electron gyrofrequency are given by

$$f_{\rm pe} = \omega_{\rm pe}/(2\pi) \approx 8.98 \times 10^{-3}\, n_e^{1/2}(x,z)\ [{\rm MHz}] \tag{A6}$$

$$f_{\rm ce} = \Omega_{\rm ce}/(2\pi) \approx 2.80\, B(z)\ [{\rm MHz}] \tag{A7}$$

respectively.

Appendix B: Equations for Electromagnetic Rays

The ray equations for magnetoionic modes are well known [e.g., *Kimura*, 1966]. In a two-dimensional plane xz the equations for the ray are given by

$$\begin{aligned} dx/dt &= 0.3\, N\, \sin\theta\, (1 - P)/R \\ dz/dt &= 0.3\, N\, \cos\theta\, (1 + P\, \tan^2\theta)/R \\ \frac{d\theta}{dt} &= -\frac{0.3}{2RN}\frac{180}{\pi}\Big[\frac{\partial n_e}{n_e \partial x}\, Q\, \cos\theta \\ &\quad - \Big(\frac{\partial n_e}{n_e \partial z}\, Q + \frac{\partial B}{B \partial z}\, S\Big)\sin\theta\Big] \\ \frac{dN}{dt} &= -\frac{0.3}{2R}\Big[\frac{\partial n_e}{n_e \partial x}\, Q\, \sin\theta + \Big(\frac{\partial n_e}{n_e \partial z}\, Q + \frac{\partial B}{B \partial z}\, S\Big)\cos\theta\Big] \end{aligned} \tag{B1}$$

In the above the distances x and z are measured in kilometers, the time t in μs, and the unit for ray phase angle θ is degree. The factor 0.3 comes from converting the speed of light in vacuo, $c = 3 \times 10^5$ km s^{-1} to the units adopted in the present study.

As is well known, one of the equations in (B1), particularly the equation for N, is redundant. It can be replaced by the local magnetoionic dispersion relation (4). Finally, the various quantities in (B1) are given by

$$\begin{aligned} R &= 1 + \frac{T f_{\rm pe}^2 f |\cos\theta|}{2f\,(Tf - f_{\rm ce}|\cos\theta|)^2} \times \Big(1 + \frac{1 - T^2}{1 + T^2}\frac{f^2 + f_{\rm pe}^2}{f^2 - f_{\rm pe}^2}\Big) \\ P &= \frac{T f_{\rm pe}^2 f_{\rm ce} |\cos\theta|}{2N^2 f\,(Tf - f_{\rm ce}|\cos\theta|)^2} \times \Big(1 - \frac{1 - T^2}{1 + T^2}\frac{1 + \cos^2\theta}{\sin^2\theta}\Big) \\ Q &= \frac{T f_{\rm pe}^2}{f\,(Tf - f_{\rm ce}|\cos\theta|)} \end{aligned} \tag{B2}$$

$$\times\left(1+\frac{1-T^2}{1+T^2}\frac{f_{pe}^2}{f^2-f_{\rm pe}^2}\frac{f_{\rm ce}|\cos\theta|}{Tf-f_{\rm ce}|\cos\theta|)}\right)$$

$$S=\frac{2}{1+T^2}\frac{Tf_{\rm pe}^2 f_{\rm ce}|\cos\theta|}{f\,(Tf-f_{\rm ce}|\cos\theta|)^2}$$

Acknowledgments. This research is supported by the National Science Foundation under grants ATM 9616136 and OPP 9505823 to the University of Maryland. Numerical computations were carried out at the National Science Foundation San Diego Supercomputer Center under a resource grant to the University of Maryland.

Janet G. Luhmann thanks John Doug Menietti and another referee for their assistance in evaluating this paper.

References

Benson, R. F., and H. K. Wong, Low-altitude ISIS 1 observations of auroral radio emissions and their significance to the cyclotron maser instability, *J. Geophys. Res., 92,* 1218, 1987.

Brinton, H. C., J. M. Grebowsky, and L. H. Brace, The high-latitude winter *F* region at 300 km: Thermal plasma observations from AE-C, *J. Geophys. Res., 83,* 4767, 1978.

Cartwright, D. E., and P. J. Kellogg, Observations of radiation from an electron beam artificially injected into the ionosphere, *J. Geophys. Res., 79,* 1439, 1974.

Doe, R. A., M. Mendillo, J. F. Vickrey, L. J. Zanetti, and R. W. Eastes, Observations of nightside auroral cavities, *J. Geophys. Res., 98,* 293, 1993.

Doe, R. A., J. F. Vickrey, and M. Mendillo, Electrodynamic model for the formation of auroral ionospheric cavities, *J. Geophys. Res., 100,* 9683, 1995.

Ellis, G. R., The *Z* propagation hole in the ionosphere, *J. Atmos. Terr. Phys., 8,* 43, 1956.

Ergun, R.E., Linear and nonlinear wave processes in the auroral ionosphere, Ph.D. thesis, Univ. of Calif., Berkeley, 1989.

Gough, M. P., and A. Urban, Auroral beam/plasma interaction observed directly, *Planet. Space Sci., 31,* 875, 1983.

Gough, M. P., D. A. Hardy, M. R. Oberhardt, W. J. Burke, L. C. Gentile, B. McNeil, K. Bounar, D. C. Thompson, and W. J. Raitt, Correlator measurements of megahertz wave-particle interactions during electron beam operations on STS, *J. Geophys. Res., 100,* 21,561, 1995.

Horne, R. B., Propagation to the ground at high latitudes of auroral radio noise below the electron gyrofrequency, *J. Geophys. Res., 100,* 14,637, 1995.

Hughes, J. M., and J. LaBelle, The latitude dependence of auroral roar, *J. Geophys. Res., 103,* 14,911, 1998.

Inan, U. S., and T. F. Bell, The plasmapause as a VLF wave guide, *J. Geophys. Res., 82,* 2819, 1977.

Kaufmann, R. L., Electrostatic wave growth: Secondary peaks in a measured auroral electron distribution function, *J. Geophys. Res., 85,* 1713, 1980.

Kelley, M. C., *The Earth's Ionosphere: Plasma Physics and Electrodynamics,* Academic, San Diego, Calif., 1989.

Kellogg, P. J., and S. J. Monson, Radio emissions from the aurora, *Geophys. Res. Lett., 6,* 297, 1979.

Kellogg, P. J., and S. J. Monson, Further studies of auroral roar, *Radio Sci., 19,* 551, 1984.

Kimura, I., Effects of ions on whistler-mode ray tracing, *Radio Sci., 1,* 269, 1966.

LaBelle, J., and A. T. Weatherwax, Ground-based observations of LF/MF/HF radio waves of auroral origin, in *Physics of Space Plasmas,* edited by T. Chang and J. R. Jaspers, p. 223, Scientific, Cambridge, Mass., 1992.

LaBelle, J., A. T. Weatherwax, M. L. Trimpi, and R. Brittain, The spectrum of LF/MF/HF radio noise at ground level during substorms, *Geophys. Res. Lett., 21,* 2749, 1994.

LaBelle, J., M. L. Trimpi, R. Brittain, and A. T. Weatherwax, Fine structure of auroral radio emissions, *J. Geophys. Res., 100,* 21,953, 1995.

Mallinckrodt, J., A sounding rocket study of auroral electron precipitation, Ph.D. thesis, Univ. of Calif., Berkeley, 1980.

McFadden, J. P., C. W. Carlson, and M. H. Boehm, High-frequency waves generated by auroral electrons, *J. Geophys. Res., 91,* 12,079, 1986.

Melrose, D. B., Emission at cyclotron harmonics due to coalescence of *z*-mode waves, *Astrophys. J., 380,* 256, 1991.

Rodger, A. S., R. J. Moffett, and S. Quegan, The role of ion drift in the formation of ionization troughs in the mid and high-latitude ionosphere: A review, *J. Atmos. Terr. Phys., 54,* 1, 1992.

Shepherd, S. G., J. LaBelle, and M. L. Trimpi, Further investigation of auroral roar fine structure, *J. Geophys. Res., 103,* 2219, 1998a.

Shepherd, S. G., J. LaBelle, and M. L. Trimpi, The polarization of auroral radio emissions, *Geophys. Res. Lett., 24,* 3161, 1998b.

Shepherd, S. G., J. LaBelle, R. A. Doe, M. McCready, and A. T. Weatherwax, Ionospheric structure and the generation of auroral roar, *J. Geophys. Res.,* this issue.

Smith, M. S., Numerical solution of the "Ellis window" problem, *Nature Phys. Sci., 243,* 29, 1973.

Tsunoda, R. T., High-latitude *F* region irregularities: A review and synthesis, *Rev. Geophys., 26,* 719, 1988.

Weatherwax, A. T., J. LaBelle, M. L. Trimpi, and R. Brittain, Ground-based observations of radio emissions near $2f_{ce}$ and $3f_{ce}$ in the auroral zone, *Geophys. Res. Lett., 20,* 1447, 1993.

Weatherwax, A. T., J. LaBelle, M. L. Trimpi, R. A. Treumann, J. Minow, and C. Deehr, Statistical and case studies of radio emissions observed near $2f_{ce}$ and $3f_{ce}$ in the auroral zone, *J. Geophys. Res., 100,* 7745, 1995.

Willes, A. J., S. D. Bale, and Z. Kuncic, A *z*-mode electron-cyclotron maser model for bottomside ionospheric harmonic radio emissions, *J. Geophys. Res., 103,* 7017, 1998.

Winglee, R. M., and G. A. Dulk, The electron-cyclotron maser instability as a source of plasma radiation, *Astrophys. J., 307,* 808, 1986a.

Winglee, R. M., and G. A. Dulk, The electron-cyclotron maser instability as the source of solar type V continuum, *Astrophys. J., 310,* 432, 1986b.

Yoon, P. H., A. T. Weatherwax, T. J. Rosenberg, and J. LaBelle, Lower ionospheric cyclotron maser theory: A possible source of $2f_{ce}$ and $3f_{ce}$ auroral radio emissions, *J. Geophys. Res., 101,* 27,015, 1996.

Yoon, P. H., A. T. Weatherwax, and T. J. Rosenberg, On the generation of auroral radio emissions at harmonics of the lower ionospheric electron cyclotron frequency: *X*, *O*, and *Z* mode maser calculations, *J. Geophys. Res., 103,* 4071, 1998.

J. LaBelle and S. G. Shepherd, Department of Physics and Astronomy, Dartmouth College, Hanover, NH 03755.

T. J. Rosenberg, A. T. Weatherwax, and P. H. Yoon, Institute for Physical Science and Technology, University of Maryland, College Park, MD 20742. (yoonp@uap.umd.edu)

(Received February 27, 1998; revised August 21, 1998; accepted September 14, 1998.)